# DETECTION OF ARCHITECTURAL DISTORTION IN MAMMOGRAMS VIA ANALYSIS OF PHASE PORTRAITS AND CURVILINEAR STRUCTURES

Fábio J. Ayres* and Rangaraj M. Rangayyan*

* Department of Electrical and Computer Engineering, University of Calgary, Calgary, Canada

ranga@ucalgary.ca

**Abstract: Architectural distortion is a subtle abnormality that can be observed in mammograms, and is one of the earliest and most commonly missed signs of breast cancer. Computer-aided diagnosis techniques can be valuable aids to the radiologist in detecting architectural distortion. Recently, we proposed a technique for the detection and localization of architectural distortion in mammograms, based on orientation fields and phase portraits. In this paper, we propose the use of methods for the identification and analysis of curvilinear structures in mammographic images, as a means to reduce the false-positive rate of our method for the detection of architectural distortion. It is shown that the selection of curvilinear structures prior to the phase portrait modeling step effectively improves the sensitivity of the method, to about 84% at 7.8 false-positives per image.**

## Introduction: Architectural distortion

Current statistics from the National Cancer Institute of Canada [1] show that breast cancer has the highest probability of development among all cancers in women. The importance of early detection of breast cancer is evident: whereas localized cancer is associated with a five-year survival rate of 97.5%, disseminated cancer leads to a five-year survival rate of only 20.4% [2]. Mammography is the best available examination for the detection of early signs of breast cancer, and mammographic screening has been shown to be highly effective in reducing breast cancer mortality rates. However, the sensitivity of screening mammography is affected by the high volume of cases to be examined in a screening program, and by the subtle appearance of abnormalities in a mammographic image. Among the most commonly missed signs of breast cancer is architectural distortion, which is defined in the Breast Imaging Reporting and Data System (BI-RADS) [3] as follows: "The normal architecture (of the breast) is distorted with no definite mass visible. This includes spiculations radiating from a point and focal retraction or distortion at the edge of the parenchyma."

Computer-aided diagnosis (CAD) techniques could offer a cost-effective alternative to double-reading as a means of reducing errors. A CAD system could act as a second reader, prompting the radiologist to review areas in a mammogram deemed suspicious by specialized computer algorithms. Recent studies have demonstrated that CAD systems can improve a radiologist's sensitivity without a substantial increase in the recall rate [4]. Nevertheless, Baker *et al.* [5] found the sensitivity of two commercial CAD systems to be poor in detecting architectural distortion: fewer than 50% of the cases of architectural distortion presented were detected. These findings indicate the need for further research in this area, and the development of algorithms designed specifically to characterize and detect architectural distortion [6].

In this paper, we propose the use of methods for the identification and analysis of curvilinear structures (CLS) in mammographic images, as a means to reduce the false-positive rate of our method for the detection of architectural distortion [7, 8]. The method consists of five stages: orientation field extraction, curvilinear structure selection, orientation field filtering and downsampling, phase portrait modeling, and detection of sites of architectural distortion. The orientation field is extracted using a bank of real Gabor filters employed as line detectors [9]. The CLS of interest (spicules and fibrous tissue) are separated from confounding structures (pectoral muscle edge, parenchymal tissue edges, breast boundary, and noise) using the orientation field, the gradient field, and a nonmaximal suppression (NMS) technique [10]. The selected core CLS pixels and the orientation field are filtered and downsampled. The orientation field is analyzed using phase portraits, yielding three phase portrait maps: node, saddle, and spiral. The node map is further analyzed in order to detect the sites of architectural distortion. Figure 1 illustrates the proposed method.

The following sections present a discussion on each stage of processing. The results of processing mammographic images containing architectural distortion from the Mini-MIAS database [11] are presented.

## Extraction of the orientation field

Gabor filters may be used as line detectors, due to their good spatial and frequency localization. In this work, we obtain the texture orientation at each pixel through the use of a Gabor filter bank. The Gabor filter bank is composed of 180 filters evenly spaced in orientation, covering the range $[-\pi/2, \pi/2]$. The Gabor filter
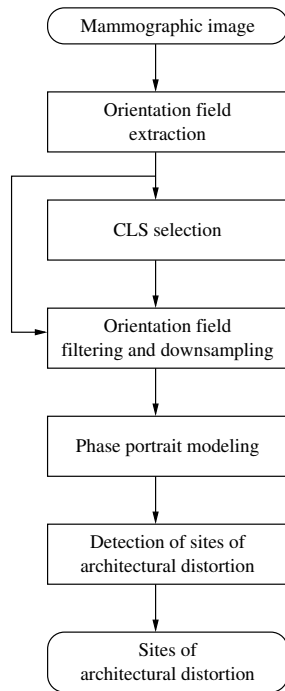
Figure 1: Block diagram of the proposed method for the detection of sites of architectural distortion in mammograms. CLS = curvilinear structure.

kernel oriented at the angle $\theta = -\pi$ is given by

$$g(x,y) = \frac{1}{2\pi\sigma_x\sigma_y}\exp\left[-\frac{1}{2}\left(\frac{x^2}{\sigma_x^2} + \frac{y^2}{\sigma_y^2}\right)\right]\cos(2\pi f x). \tag{1}$$

Rotation of this kernel allows the generation of Gabor kernels at different angles. In the present work, the parameters in Equation (1), namely $\sigma_x$, $\sigma_y$, and $f$, are derived from design rules as follows:

- Let $\tau$ be the full-width at half-maximum of the Gaussian term in Equation (1) along the $x$ axis. Then, $\sigma_x = \tau/(2\sqrt{2\ln 2}) = \tau/2.35$.
- The cosine term has a period of $\tau$; therefore, $f = 1/\tau$.
- The value of $\sigma_y$ is defined as $\sigma_y = l\sigma_x$, where $l$ determines the elongation of the Gabor filter in the $y$ direction, as compared to the extent of the filter in the $x$ direction.

We use $\tau = 4$ pixels (corresponding to a thickness of 0.8 $mm$ at a pixel size of 200 $\mu m$) and $l = 8$ in the present work. These values were determined empirically, by observing the typical spicule width and length in mammograms with architectural distortion in the Mini-MIAS database [11].

The texture orientation at a pixel is estimated as the orientation of the Gabor filter that yields the highest magnitude response at that pixel. The orientation at every pixel is used to compose the orientation field angle $\theta(x,y)$. The magnitude of the corresponding filter re-

sponse forms the magnitude image $M(x,y)$. The orientation field thus obtained has the same resolution as the original mammogram (200 $\mu m$).

## Curvilinear structure selection

The Gabor filter bank described above is sensitive to line structures, such as spicules and fibers. However, the filter bank also recognizes strong image edges as oriented features. Examples of strong edges in mammographic images are the pectoral muscle edge, the parenchymal tissue edge, and vessel walls. Strong edges around the fibro-glandular disk may be of interest in the detection of focal retraction, a particular form of architectural distortion [6]. Nevertheless, in our method, it is desirable that only linear structures related to fibro-glandular tissue are identified as oriented features.

The method for the selection of CLS implemented in this work includes three stages: segmentation of the breast area, detection of core CLS pixels, and rejection of CLS pixels at sites with a strong gradient.

The breast area is segmented by the thresholding method of Otsu [12]. Pixels outside the breast area are removed from further consideration at this stage. The core CLS pixels are detected using the NMS technique [10] applied to the magnitude image. The NMS algorithm identifies the core CLS pixels by comparing each pixel in the magnitude image with its neighbors along the direction that is perpendicular to the local orientation field angle. If the pixel under investigation has a larger magnitude value than the corresponding neighbors, the pixel is considered to be a core CLS pixel. Nonmaximal suppression is a common step in many edge detectors (e.g., Canny [13]), and Zwiggelaar *et al.* [14] used NMS, as described in this section, for the detection of CLS pixels.

The core CLS pixels associated with the presence of strong gradients are rejected. The rejection procedure implemented in this work follows the pixel rejection criteria proposed by Karssemeijer and te Brake [15], in the context of detection of spiculated lesions. The gradient of the mammographic image is obtained using the first derivative of a Gaussian with a standard deviation of 1$mm$. The direction of the gradient is computed, and compared to the direction of the orientation field, for each core CLS pixel. The core CLS pixel is discarded if the difference between the direction of the orientation field and the direction perpendicular to the gradient is less than $\pi/6$. It is assumed that the presence of a strong gradient causes a ripple in the magnitude image, leading to an erroneous detection of a CLS.

Curvilinear structures present within the fibro-glandular disk will exhibit reduced contrast as compared to similar CLS outside the fibro-glandular disk. As a consequence, CLS within the fibro-glandular disk will present smaller magnitude field values than those of CLS outside the fibro-glandular disk. In order to assign the same weight to all CLS, independent of location, the magnitude field $M(x,y)$ is replaced by an image com-

posed of the core CLS pixels, $M_{CLS}(x,y)$, defined as follows:

$$M_{CLS}(x,y) = \begin{cases} 1 & \text{if pixel at } (x,y) \text{ is core CLS pixel} \\ 0 & \text{otherwise.} \end{cases}$$
(2)

This procedure ensures that important CLS with low contrast, such as spicules within the fibro-glandular disk, are not missed by the algorithm.

**Filtering and downsampling the orientation field**

It is necessary to downsample the orientation field in order to reduce the computational effort required to process full mammograms. The downsampling procedure must be preceded by a filtering step in order to avoid the loss of important information regarding the presence of CLS, and to reduce noise.

Let $h(x,y)$ be a Gaussian filter of standard deviation $\sigma_f$, defined as

$$h(x,y) = \frac{1}{2\pi\sigma_f} \exp\left[-\frac{1}{2}\left(\frac{x^2+y^2}{\sigma_f^2}\right)\right].$$
(3)

Define the images $s(x,y) = M_{CLS}(x,y)\sin[2\theta(x,y)]$ and $c(x,y) = M_{CLS}(x,y)\cos[2\theta(x,y)]$. Then, the filtered orientation field angle $\theta_f(x,y)$ is obtained as

$$\theta_f(x,y) = \frac{1}{2}\arctan\left(\frac{(h*s)(x,y)}{(h*c)(x,y)}\right),$$
(4)

where the asterisk denotes convolution.

The filtered orientation field angle is downsampled by a factor of four, thus producing the downsampled orientation field angle $\theta_d$ as

$$\theta_d(x,y) = \theta_f(4x,4y).$$
(5)

The magnitude $M_{CLS}(x,y)$ of the orientation field is also filtered and downsampled. The filtered orientation field magnitude $M_f(x,y)$ is given by

$$M_f(x,y) = (h*M_{CLS})(x,y),$$
(6)

and the downsampled magnitude field is given by

$$M_d(x,y) = M_f(4x,4y).$$
(7)

The resulting angle and magnitude fields have a resolution of 0.8 *mm*/pixel. The angle filtering procedure employed in this work is a variant of Rao's dominant local orientation method [16]: in our procedure we use a Gaussian filter instead of a box filter.

**Phase portrait modeling**

The phase portrait of a system of differential equations is the display of the possible trajectories, in the phase plane, of the state of a dynamical system. Rao and Jain [16, 17] have employed phase portraits to analyze

images depicting oriented texture patterns as follows: the geometrical patterns in phase portraits of systems of two linear first-order differential equations are associated with the patterns encountered in an image presenting oriented texture. Recently, we used phase portrait modeling to detect architectural distortion in mammograms [7, 8]: the present work is an extension of our previous method.

Consider the following system of linear first-order differential equations:

$$\begin{pmatrix} \dot{p}(t) \\ \dot{q}(t) \end{pmatrix} = \mathbf{A}\begin{pmatrix} p(t) \\ q(t) \end{pmatrix} + \mathbf{b},$$
(8)

where $\mathbf{A}$ is a $2 \times 2$ matrix and $\mathbf{b}$ is a $2 \times 1$ column matrix (a vector). The functions $p(t)$ and $q(t)$ represent the state variables of a dynamical system, as a function of time (e.g., the position and the momentum of a particle, or the pressure and the temperature of a gas). In this case, there are only three possible types of phase portraits: node, saddle, and spiral [18]. The type of phase portrait can be determined from the nature of the eigenvalues of $\mathbf{A}$. The center $(p_0, q_0)$ of the phase portrait is given by the *fixed point* of Equation (8):

$$\begin{pmatrix} \dot{p}(t) \\ \dot{q}(t) \end{pmatrix} = 0 \Rightarrow \begin{pmatrix} p_0 \\ q_0 \end{pmatrix} = -\mathbf{A}^{-1}\mathbf{b}.$$
(9)

Associating the functions $p(t)$ and $q(t)$ with the $x$ and $y$ coordinates of the Cartesian (image) plane, we can define the *orientation field* generated by Equation (8) as

$$\phi(x,y|\mathbf{A},\mathbf{b}) = \arctan\left(\frac{\dot{q}(t)}{\dot{p}(t)}\right),$$
(10)

which is the angle of the velocity vector $[\dot{p}(t), \dot{q}(t)]$ with the $x$ axis at $(x,y) = [p(t), q(t)]$. Using the concepts presented above, we may qualitatively describe the orientation field of a textured image by determining locally the type of the phase portrait that is most similar to the orientation field, along with the center of the phase portrait. This notion will be employed in the present work to detect and localize architectural distortion, as described below.

An analysis window of $10 \times 10$ pixels ($8 \times 8$ *mm*) is slid pixel by pixel through the downsampled orientation field. The phase portrait model parameters [the matrix $\mathbf{A}$ and the vector $\mathbf{b}$ in Equation (8)] that best represent the orientation field under the analysis window are estimated, at each position of the analysis window. In order to estimate $\mathbf{A}$ and $\mathbf{b}$, let $\Delta(x,y|\mathbf{A},\mathbf{b})$ be a measure of the error between the downsampled orientation field $\theta_d(x,y)$ and the orientation $\phi(x,y|\mathbf{A},\mathbf{b})$ given by the model, at the pixel location $(x,y)$. The error measure is defined as

$$\Delta(x,y|\mathbf{A},\mathbf{b}) = M_d(x,y)\sin[\theta_d(x,y) - \phi(x,y|\mathbf{A},\mathbf{b})]. \quad (11)$$

The sum of the squared error is given by

$$\varepsilon^2(\mathbf{A},\mathbf{b}) = \sum_x \sum_y \Delta^2(x,y|\mathbf{A},\mathbf{b}),$$
(12)

where the range of the summation indexes $x$ and $y$ is the set of the pixel locations within the analysis window. Estimates of $\mathbf{A}$ and $\mathbf{b}$ that minimize $\varepsilon^2(\mathbf{A},\mathbf{b})$ are obtained as follows:

(1) Initial estimates $\mathbf{A_{SA}}$ and $\mathbf{b_{SA}}$ of $\mathbf{A}$ and $\mathbf{b}$ are obtained through the minimization of $\varepsilon^2(\mathbf{A},\mathbf{b})$ using simulated annealing [19].
(2) A nonlinear least squares algorithm [20] is used to refine the estimates $\mathbf{A_{SA}}$ and $\mathbf{b_{SA}}$ obtained in the previous step, producing the optimal estimates $\mathbf{A_{opt}}$ and $\mathbf{b_{opt}}$.

The type of phase portrait is determined by the eigenvalues of $\mathbf{A_{opt}}$; the fixed point location is given by Equation (9), using the optimal values $\mathbf{A_{opt}}$ and $\mathbf{b_{opt}}$. A vote is cast in the corresponding phase portrait map, at the fixed point location. This process is repeated for every position of the analysis window.

### Detection of sites of architectural distortion

The node map is used to detect and locate the sites of architectural distortion in a mammogram, as follows:

(1) A Gaussian filter of standard deviation equal to 4.8 *mm* (6 pixels) is applied to the node map in order to reduce noise.
(2) The filtered node map is processed with a morphological gray-scale opening procedure with a structuring element of radius 8 *mm* (10 pixels) to eliminate peaks in the filtered node map that are closer than 8 *mm* to a locally dominant peak.
(3) The peaks of the resulting image are detected, and a threshold is applied to eliminate false positives. The remaining peaks, if any, indicate the potential sites of architectural distortion.

### Results

The proposed method was applied to 19 mammograms containing architectural distortion, from the Mini-MIAS database [11]. For comparison purposes, a modified version of the proposed method, in which the CLS selection step is removed, was also applied to the same mammograms. The removal of the CLS selection stage was accomplished by the following modifications:

- skipping the NMS step and the rejection of core CLS pixels associated with strong gradients, and
- setting all pixels in $M_{CLS}(x,y)$ to one.

Figure 2 shows a mammographic image in which architectural distortion is present. The magnitude image $M(x,y)$ is shown in Figure 3. Observe that the magnitude image presents a higher response for CLS located outside the fibro-glandular disk, due to their higher contrast as compared to CLS within the fibro-glandular disk.

The rejection of core CLS pixels associated with strong gradients is illustrated in Figure 4. The figure displays a region of interest (ROI) from the mammographic image in Figure 2, which contains a blood vessel. It is noticed that some of the rejected core CLS pixels are associated with the walls of the vessel. Several other rejected core CLS pixels are not associated with the displayed vessel. This observation indicates the need for improved methods for CLS selection.

The usage of CLS selection improved the specificity of our algorithm for the detection of architectural distortion, when compared with the same method without CLS selection. This observation is supported by the results shown in Figures 5 and 6. Figure 5 shows the filtered node map obtained without and with CLS selection. It is observed that the node map with CLS selection exhibits a single strong response at the site of architectural distortion. The node map without CLS selection is characterized by a strong response at the site of architectural distortion, as well as a strong response in the nipple region, and scattered responses throughout the breast area. The CLS selection step eliminates pixels that do not convey relevant information in the context of detecting architectural distortion. This increase in the quality of available information improves the meaningfulness of the estimated parameters in the phase portrait modeling step, resulting in more specific detection of architectural distortion.

Figure 6 shows the free-response receiver operating characteristics (FROC) curve for the proposed method, as well as the FROC curve obtained without CLS selection. It is observed that the use of CLS selection results in a more sensitive detection algorithm, with fewer false positives per image, when compared to the same method without CLS selection.

### Discussion

In this work, we proposed the use of CLS analysis to improve the specificity of our method for the detection of architectural distortion in mammograms. A significant improvement in specificity was obtained; nevertheless, further reduction in the number of false-positives is required. Improved methods for the detection of architectural distortion at low false-positive rates should lead to efficient and earlier detection of breast cancer.

### Acknowledgments

### References

[1] NATIONAL CANCER INSTITUTE OF CANADA. Canadian cancer statistics 2004, 2004. Available at
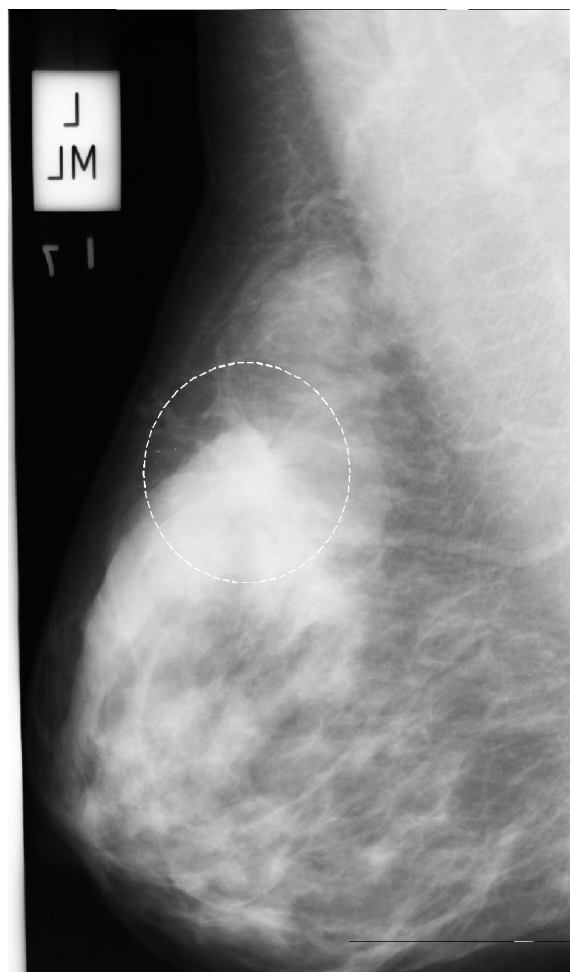
Figure 2: Mammographic image (mdb115 from the Mini-MIAS database) exhibiting architectural distortion (dashed circle).
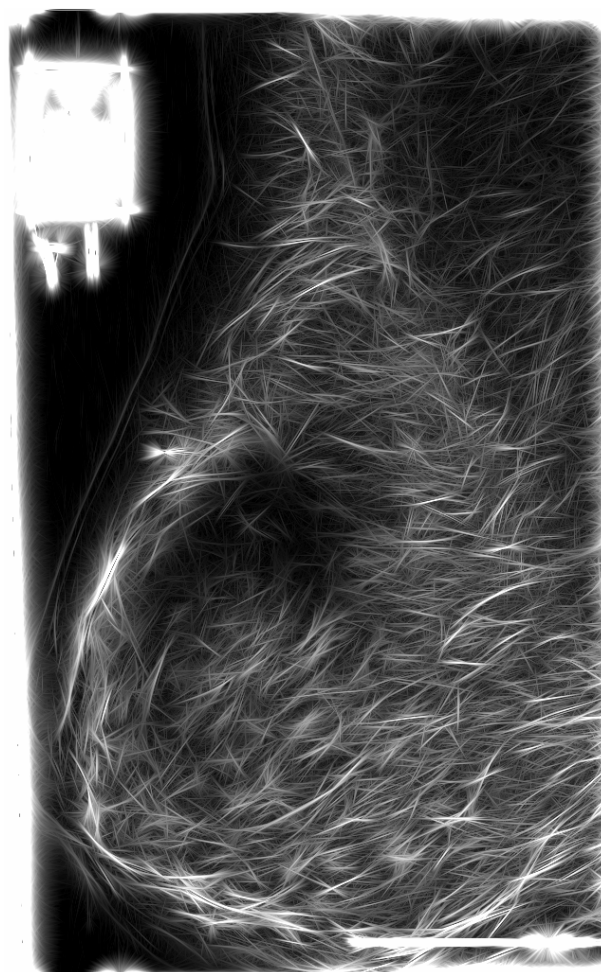


Figure 3: Magnitude image from the Gabor filter bank for the mammogram in Figure 2.
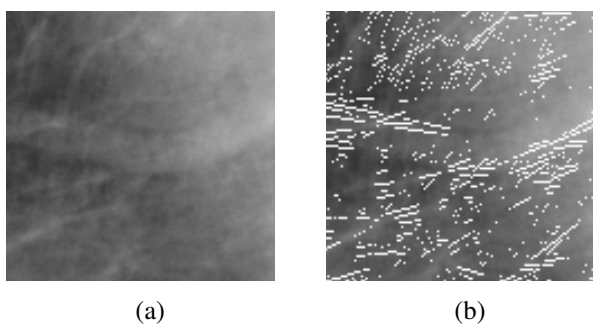


(a)            (b)

Figure 4: Rejection of core CLS pixels associated with strong gradients. (a) Region-of-interest (ROI) from the mammographic image in Figure 2. (b) Rejected pixels (shown in white) superimposed on the ROI in (a).
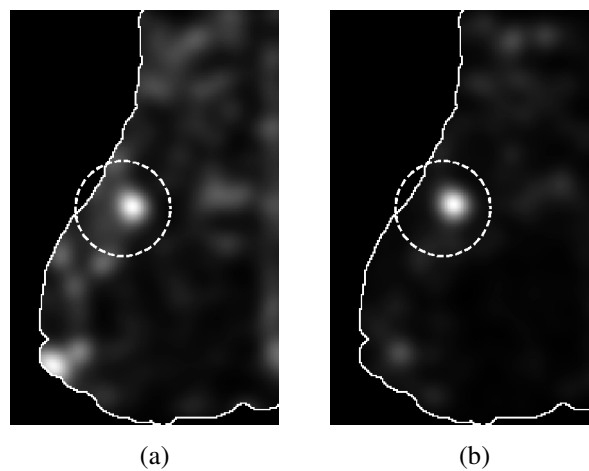


(a)            (b)

Figure 5: Node map for the mammogram in Figure 2 after Gaussian filtering ($\sigma = 4.8$ *mm*): (a) without CLS selection; (b) using CLS selection. Dashed circle: site of architectural distortion.
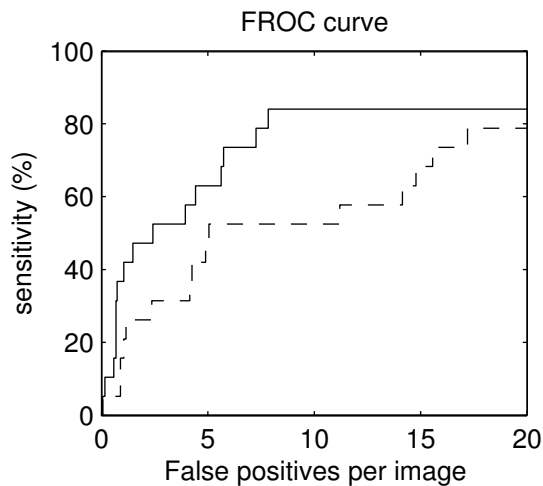
## FROC curve



Figure 6: Comparison of FROC curves obtained with and without CLS selection. Solid line: with CLS selection. Dashed line: without CLS selection.

http://www.cancer.ca/vgn/images/portal/cit_86751114/14/33/195986411niw_stats2004_en.pdf, accessed on Feb 10, 2005.

[2] A. JAMAL, L. X. CLEGG, E. WARD, L. A. G. RIES, X. WU, P. M. JAMISON, P. A. WINGO, H. L. HOWE, R. N. ANDERSON, and B. K. EDWARDS. Annual report to the nation on the status of cancer, 1975-2001, with a special feature regarding survival. *Cancer*, 101(1):3–27, 2004.

[3] AMERICAN COLLEGE OF RADIOLOGY (ACR). *Illustrated breast imaging reporting and data system (BI-RADS)*. American College of Radiology, Reston, VA, 3rd edition, 1998.

[4] S. M. ASTLEY and F. J. GILBERT. Computer-aided detection in mammography. *Clinical Radiology*, 59:390–399, 2004.

[5] J. A. BAKER, E. L. ROSEN, J. Y. LO, E. I. GIMENEZ, R. WALSH, and M. S. SOO. Computer-aided detection (CAD) in screening mammography: Sensitivity of commercial CAD systems for detecting architectural distortion. *American Journal of Röentgenology*, 181:1083–1088, 2003.

[6] T. ICHIKAWA, T. MATSUBARA, T. HARA, H. FUJITA, T. ENDO, and T. IWASE. Automated detection method for architectural distortion areas on mammograms based on morphological processing and surface analysis. In J. M. Fitzpatrick and M. Sonka, editors, *Proceedings of SPIE Medical Imaging 2004: Image Processing*, pages 920–925, San Diego, CA, February 2004. SPIE.

[7] F. J. AYRES and R. M. RANGAYYAN. Characterization of architectural distortion in mammograms. *IEEE Engineering in Medicine and Biology Magazine*, pages 59–67, January 2005.

[8] F. J. AYRES and R. M. RANGAYYAN. Detection of architectural distortion in mammograms using phase portraits. In J. M. Fitzpatrick and

M. Sonka, editors, *Proceedings of SPIE Medical Imaging 2004: Image Processing*, volume 5370, pages 587–597, San Diego, CA, February 2004.

[9] B. S. MANJUNATH and W. Y. MA. Texture features for browsing and retrieval of image data. *IEEE Transactions on Pattern Analysis and Machine Intelligence*, 18(8):837–842, 1996.

[10] M. SONKA, V. HLAVAC, and R. BOYLE. *Image Processing, Analysis and Machine Vision*. Chapman & Hall, London, England, 1st edition, 1993.

[11] J. SUCKLING, J. PARKER, D. R. DANCE, S. ASTLEY, I. HUTT, C. R. M. BOGGIS, I. RICKETTS, E. STAMAKIS, N. CERNEAZ, S.-L. KOK, P. TAYLOR, D. BETAL, and J. SAVAGE. The Mammographic Image Analysis Society Digital Mammogram Database. In A. G. Gale, S. M. Astley, D. D. Dance, and A. Y. Cairns, editors, *Digital Mammography: Proceedings of the 2nd International Workshop on Digital Mammography*, pages 375–378, York, England, July 1994. Elsevier.

[12] N. OTSU. A threshold selection method from gray-level histograms. *IEEE Transactions on Systems, Man, and Cybernetics*, 9(1):62–66, 1979.

[13] J CANNY. A computational approach to edge detection. *IEEE Transaction on Pattern Analysis and Machine Intelligence*, 8(6):679–698, 1986.

[14] R. ZWIGGELAAR, S. M. ASTLEY, C. R. M. BOGGIS, and C. J. TAYLOR. Linear structures in mammographic images: Detection and classification. *IEEE Transactions on Medical Imaging*, 23(9):1077–1086, September 2004.

[15] N. KARSSEMEIJER and G. M. TE BRAKE. Detection of stellate distortions in mammograms. *IEEE Transactions on Medical Imaging*, 15(5):611–619, 1996.

[16] A. R. RAO. *A Taxonomy for Texture Description and Identification*. Springer-Verlag, New York, NY, 1990.

[17] A. R. RAO and R. C. JAIN. Computerized flow field analysis: Oriented texture fields. *IEEE Transactions on Pattern Analysis and Machine Intelligence*, 14(7):693–709, July 1992.

[18] C. R. WYLIE and L. C. BARRETT. *Advanced Engineering Mathematics*. McGraw-Hill, New York, NY, 6th edition, 1995.

[19] S. KIRKPATRICK, C. D. GELATT, and M. P. VECCHI. Optimization by simulated annealing. *Science*, 220(4598):671–680, 1983.

[20] N. GERSHENFELD. *The Nature of Mathematical Modeling*. Cambridge University Press, Cambridge, UK, 1999.